Nonlinear Adaptive Filters for Speckle Suppression in Ultrasonic Images

Eleftherios Kofidis [*]   Sergios Theodoridis [†]   Constantine Kotropoulos [‡]

Ioannis Pitas [‡]

Correspondence address:

Prof. S. Theodoridis

Department of Informatics,

Division of Communications and Signal Processing,

University of Athens, Panepistimioupolis, Athens 157 71, Greece.

E-mail: stheodor@di.uoa.gr

Fax: +30-01-7219561

[*]Department of Computer Engineering and Informatics, University of Patras, Patras 265 00, Greece.

[†]Department of Informatics, Division of Communications and Signal Processing, University of Athens, Athens 157 71, Greece, and Computer Technology Institute, Patras 261 10, Greece.

[‡]Department of Informatics, University of Thessaloniki, Thessaloniki 540 06, Greece.

1

No. pages: 36

No. tables: 3

No. figures: 12

Abstract

A novel approach to suppression of ultrasonic speckle based on a combination of segmentation and optimum L-filtering is presented. With the aid of a suitable modification of the Learning Vector Quantizer (LVQ) neural network, the image is segmented in regions of (approximately) homogeneous statistics. For each of the regions a minimum mean-squared-error (MMSE) L-filter is designed, by using the histogram of grey levels as an estimate of the parent distribution of the noisy observations and a suitable estimate of the (assumed constant) original signal in the corresponding region. Thus, a bank of L-filters results, with each of them corresponding to and operating on a different image region. Simulation results from both simulated and real B-mode ultrasonic images are presented, which verify the (qualitative and quantitative) superiority of our technique over a number of commonly used speckle filters.

1   Introduction

Ultrasonic imaging has become an important modality in the field of medical imaging systems [18, 6] mainly because of the nonionizing nature of the ultrasonic radiation, which minimizes the risk to both patient and examiner and the unique properties of acoustical imagery which render it complementary to other diagnostic tools. Studying ultrasonic images can help not only in estimating the boundaries of organs or lesions but also in the so-called tissue characterization, that is, understanding tissue details by the appearance of the corresponding image texture [33]. However, ultrasonic (US) images suffer from a special kind of noise, called "speckle", which has its source in the scattering of the ultrasonic pulse from microscopic tissue inhomogeneities. Speckle generation is modeled as a random walk in the complex plane and in the case of a large number of scatterers within the resolution cell (fully-developed speckle) the real and imaginary parts of the resulting complex field are Gaussian random variables. Thus, the envelope detected signal (amplitude) is Rayleigh distributed and the corresponding intensity (amplitude squared) obeys negative exponential statistics [2, 5]. The fact that speckle follows a Rayleigh distribution implies that the signal-to-noise ratio, which we define as the ratio of the mean to the standard deviation of the envelope, equals 1.91, a low value which reflects the importance of this noise source [18]. A multiplicative model for the noise is implied by the fact that the standard deviation is directly proportional to the mean and

it has been verified experimentally [13].[1] The poor quality of the US images, due to speckle artifacts, degrades their clinical information content, preventing accurate diagnosis. Experimental results reported in [24] indicated that, although the resolution of the imaging system is the limiting factor for the detection of high-contrast lesions, it is the speckle noise that limits the detection of low-contrast lesions.

Several algorithms have been proposed aiming at reducing speckle noise in images (e.g., [3, 13, 16, 19, 15, 34]). Since the ultimate goal of any speckle suppression scheme should be the reduction of speckle contrast to enhance the diagnostic value of the image, edge and detail preservation are crucial in a speckle filter along with noise reduction. Thus, spatially-varying filters are required that are also able to deal with the *nonlinear* model governing the degradation process [22].

An important class of adaptive speckle filters is what we call here "segmentation-based filters", that is, filtering processes combining segmentation and (nonadaptive) filters. The underlying idea is that, with the aid of a suitable segmentation algorithm, a statistically nonstationary image can be divided into approximately stationary regions which can, in turn, be processed by filters designed on the basis of the corresponding statistics. Thus, we have a set of filters with each of them corresponding to and operating on a different region of the image, with the various regions being dictated by the segmentation result. The idea of transforming an image into a set of statistically stationary subimages and feeding these to (nonadaptive) filtering processes is not new. It has been applied in the past to image restoration and compression [23, 27]. In this paper, we present such an approach to speckle suppression (recently introduced [8]) employing a modification of the Learning Vector Quantizer neural network at the segmentation stage and nonadaptive minimum mean-squared error (MMSE) L-filters at the filtering stage, designed with the ordering statistical information acquired from the segmentation stage. The proposed filters are tested on a B-mode image of a tissue simulating phantom as well as a real liver image and the results compare favorably to those produced by a single L-filter designed with the sample statistics of the image considering this as statistically homogeneous. Results of comparison with a number of commonly used

---

[1]Nevertheless, it must be mentioned that speckle noise is only approximately multiplicative in regions of the object containing fine details that cannot be resolved by the imaging system [30] and the experimental verification in [13] was based only on flat areas of the image. In spite of this, speckle noise is usually modeled as multiplicative in practice.

speckle filters are also given, which rank our method among the first positions. The noise-smoothing performances of the various filters are compared on the basis of the resulting receiver operating characteristics (ROC's) and an SNR quantity measuring the dispersion of the image pixels in the lesion and background regions from the corresponding true means. The contrast enhancement effect of the filters is quantitatively assessed through a lesion contrast measure. We also present the results of subtracting the SNR image of the original scan from the filtered ones, an operation that improves the lesion detectability. Finally, an example is given to demonstrate the effect of speckle suppression on the edge detection task.

The paper is organized as follows. Our method is presented in detail in Section 2. Experimental results from the application of the proposed filters to a simulated and a real B-scan are included in Section 3, along with a comparison with a number of other well known filtering strategies. Some implementation issues are discussed in Section 4, which concludes the paper.

2   Segmentation-Based L-Filtering

In this section we present an adaptive nonlinear approach to speckle suppression in US B-mode images. The adaptivity of our method comes from the fact that the image is first segmented into regions of different tissue and lesion characteristics and each of the resulting regions is processed by a different filter. L-filters are employed to deal with the nonlinear nature of the noise. A number of approaches to the segmentation of speckle images have been reported (e.g., [14]). A recently introduced segmentation technique, that we have adopted in this work, employs a modification of a well known self-organizing neural network, the Learning Vector Quantizer (LVQ), based on the L_2 mean which has been shown to be more suitable for US images [11]. A block diagram illustrating the idea of the proposed method is shown in Fig. 1.

In the sequel, a brief presentation of LVQ is given followed by the description of its modification, L_2 LVQ, along with a discussion of the need for this modified form. The derivation of the MMSE L-filter for the case of a known constant signal corrupted by noise is included both in the unconstrained and constrained (unbiased) cases. In most cases it is unrealistic to assume that the signal is constant. However, since the filters are matched to specific regions of the image, this simplifying assumption is a good approximation of the reality for practical purposes.

2.1 The Learning Vector Quantizer and its L_2 Mean Based Modification

Learning Vector Quantizer (LVQ) [9] is a self-organizing neural network (NN) that belongs to the so-called competitive NN's. It implements a nearest-neighbor classifier using an error correction encoding procedure that could be characterized as a stochastic approximation version of K-means clustering. In this subsection, we briefly present the LVQ algorithm and its modification based on the L_2 mean (L_2 LVQ) along with a discussion of the reasons that make L_2 LVQ suitable for our application.

Let us first present the basic idea. As in the Vector Quantization (VQ) problem, we have a finite set of variable reference vectors (or "codevectors" in the VQ terminology) $\{\mathbf{w}_i(t); \mathbf{w}_i \in \mathcal{R}^N, i = 1, 2, \ldots, p\}$ and a set of training vectors $\mathbf{x}(t) \in \mathcal{R}^N$ where t denotes time and we wish to classify the training vectors into p classes represented by the vectors $\mathbf{w}_i$. These representative vectors are obtained by following an iterative procedure where at each iteration step t the current feature vector $\mathbf{x}(t)$ is compared to all the $\mathbf{w}_i(t)$ and the best-matching $\mathbf{w}_i(t)$ is updated to better comply with $\mathbf{x}(t)$. In this way, in the long run, the different reference vectors tend to become specifically tuned to different domains of the input $\mathbf{x}$. The learning stage of the algorithm is described in the following 4-step procedure:

1. Initialize randomly the reference vectors $\mathbf{w}_i(0)$, $i = 1, 2, \ldots, p$.

2. At time step t, find the "winner" class c such that:
$$\|\mathbf{x}(t) - \mathbf{w}_c(t)\| = \min_i \{\|\mathbf{x}(t) - \mathbf{w}_i(t)\|\}. \tag{1}$$

3. Update the winner:
$$\mathbf{w}_c(t+1) = \mathbf{w}_c(t) + \alpha(t)(\mathbf{x}(t) - \mathbf{w}_c(t)). \tag{2}$$

4. Repeat steps 2 and 3 until convergence.

The gain factor $\alpha(t)$ is a scalar parameter ($0 < \alpha < 1$) which should be a decreasing function of time in order to guarantee the convergence to a unique limit. In the recall procedure, the class with which the input vector $\mathbf{x}(t)$ is most closely associated is determined as in (1) where now $\mathbf{w}_i$ is the i-th reference vector after the convergence of the learning procedure[2].

---

[2]To be precise, we should note that the algorithm described above is the "single-winner" version of LVQ. In its general "multiple-winner" form, step 3 above involves updating not only the winner vector but its neighbors as well with the neighborhood defined either in a topological [9] or in a vectorial distance [7] sense. This general form of LVQ has been applied with success to the segmentation of MR images [26].

It is easy to see that eq. (2) above is in fact a recursive way of computing the average of the training vectors classified to the class c (this is easily verified by choosing $\alpha(t) = 1/(t+1)$). Thus, after the end of the learning phase, the reference vectors will correspond to the centroids of the associated classes. It has been shown both analytically and by simulations and experimental B-scans, that, in the case of the so-called "fully-developed speckle", i.e., when the density of the scatterers within the insonified medium is large enough, the second and higher order speckle statistics are independent of the tissue characteristics [20]. In other words, the mean echo amplitude level sufficiently characterizes the statistical content of the US image, as far as the detection of lesion against the background is concerned. These remarks explain well enough why LVQ, despite its simplicity, is sufficient for a US image segmentation task.

However, it should be noted that the arithmetic mean approximated by the basic LVQ, described so far, is not the best possible estimator of the mean level in a US image. It has been proved [12] that the maximum likelihood estimator of the original noiseless image is the L_2 mean [22] (scaled by $\frac{\sqrt{\pi}}{2}$) of the noisy observations x_i, $i = 1, \ldots, M$, i.e.,

$$\frac{\sqrt{\pi}}{2} \sqrt{\frac{1}{M} \sum_{i=1}^{M} x_i^2}. \tag{3}$$

This result leads us to consider a modification of the standard LVQ algorithm, in which the reference vectors correspond to the L_2 mean instead of the arithmetic mean. The learning and recall parts of the modified algorithm, which we call L_2 LVQ, are exactly analogous to those of the standard LVQ except that the elements of the reference and input vectors are replaced by their squares. This simple modification allows for the computation of the L_2 means providing us at the same time with an algorithm that is proven to be convergent in the mean and in the mean square sense [11].

2.2 MMSE L-Filter Design for a Known Constant Signal Embedded in Noise

The L-filter [1], defined as a linear combination of the input order statistics, has some distinct advantages, making it a right choice for tasks such as the one treated here: it can cope with nonlinear models, it has a relatively simple MMSE design, and furthermore it performs at least as well as, for example, the mean and the median filters, as it includes these filters as special cases [1].

In the sequel, s denotes the constant and known signal, which is corrupted by white[3] noise, independent of s, yielding the noisy observation x. The output of the L-filter of length M is given by:

$$y = \mathbf{a}^T \mathbf{x} \tag{4}$$

where $\mathbf{a} = (a_1, a_2, \ldots, a_M)^T$ is the L-filter coefficient vector and $\mathbf{x} = (x_{(1)}, x_{(2)}, \ldots, x_{(M)})^T$ is the vector of the observations arranged in ascending order of magnitude (i.e., order statistics). We will design the optimum in the mean-squared error (MSE) sense L-filter, that is, determine the vector $\mathbf{a}$ minimizing $E\{(s - y)^2\}$. By using (4) we obtain:

$$E\{(s - y)^2\} = E\{s^2 + \mathbf{a}^T \mathbf{x} \mathbf{x}^T \mathbf{a} - 2s\mathbf{a}^T \mathbf{x}\} \tag{5}$$

or

$$E\{(s - y)^2\} = s^2 + \mathbf{a}^T \mathbf{R} \mathbf{a} - 2s\mathbf{a}^T \boldsymbol{\mu} \tag{6}$$

where $\mathbf{R} = E\{\mathbf{x}\mathbf{x}^T\}$ is the autocorrelation matrix of the vector of the ordered observations and $\boldsymbol{\mu} = E\{\mathbf{x}\} = (E\{x_{(1)}\}, E\{x_{(2)}\}, \ldots, E\{x_{(M)}\})^T$ is the vector of the expected values of these observations. Setting the derivative of (6) with respect to $\mathbf{a}$ equal to zero yields the following expression for the optimum coefficient vector:

$$\mathbf{a} = s\mathbf{R}^{-1}\boldsymbol{\mu} \tag{7}$$

It remains to compute the ordering statistics $\boldsymbol{\mu}$ and $\mathbf{R}$. Expressions for the evaluation of these quantities are given in [1] and involve the calculation of the marginal and bivariate probability density functions (pdf's) of the ordered input given its parent distribution:

$$E\{x_{(i)} x_{(j)}\} = \int\int xy f_{x_{(i)} x_{(j)}}(x, y) dx dy \quad (i < j) \tag{8}$$

$$E\{x_{(i)}\} = \int x f_{x_{(i)}}(x) dx \tag{9}$$

where

$$f_{x_{(i)}}(x) = K_i F_x^{i-1}(x) [1 - F_x(x)]^{M-i} f_x(x) \tag{10}$$

$$f_{x_{(i)} x_{(j)}}(x, y) = K_{i,j} F_x^{i-1}(x) [F_x(y) - F_x(x)]^{j-i-1}$$
$$\times [1 - F_x(y)]^{M-j} f_x(x) f_x(y) \tag{11}$$

---

[3]In fact, speckle noise is locally correlated. Smith et al. [25] argue that, for the observations to be independent, they must belong to different speckle correlation cells. Since our purpose is to apply filters scanning the image in raster fashion, such a recommendation cannot be used directly, thus the whiteness assumption is made to approximate the real situation.

and

$$K_i \quad = \quad \frac{M!}{(i-1)!(M-i)!} \tag{12}$$

$$K_{i,j} \quad = \quad \frac{M!}{(i-1)!(j-i-1)!(M-j)!} \tag{13}$$

Notice that when we are dealing with digital images, the above random variables are of discrete type. Thus, the integrals in eqs. (8), (9) are in fact discrete sums.

The minimization of the MSE subject to the constraint that $\mathbf{a}$ provides an unbiased estimate of s, i.e.,

$$s = E\{y\} = \mathbf{a}^T \boldsymbol{\mu}, \tag{14}$$

is performed as in the case of additive noise [1] yielding the expression

$$\mathbf{a} = \frac{s\mathbf{R}^{-1}\boldsymbol{\mu}}{\boldsymbol{\mu}^T \mathbf{R}^{-1}\boldsymbol{\mu}} \tag{15}$$

for the coefficient vector of the unbiased L-filter.

3   Experimental Results

We have first applied our algorithm to a simulated US B-mode image, shown in Fig. 2a. It is the B-scan of a tissue mimicking phantom of size 4 cm×4 cm, with a circular (disk) lesion in the middle of diameter 2 cm [32]. The density of scatterers is 5000 cm^{-3} and the echo amplitude in the lesion area is 5 dB higher than that in the background. The image has dimensions 241×241. Its resolution is of 6 bits/pixel. However, for better visualization, the images presented here were expanded to the range 0 to 255 before being displayed. Because of the high scatterer density, the image of Fig. 2a is an example of fully developed speckle. The histograms of the lesion and background regions are plotted in Fig. 2b. They are seen to be quite similar to Rayleigh probability density functions.

Fig. 3 shows the result of the segmentation of the original image. Two image regions having different L_2 means have been determined. The dark pixels correspond to the background, while the bright ones to the lesion area. For the classification of the image pixels into two groups, we have employed the L_2 LVQ algorithm with parameters $p = 2$ and $N = 49$, trained on a large set of pattern vectors that have been produced by a raster scanning of the image with a 7×7 window.

The histograms of the two regions of the original image classified as dark and bright in Fig. 3 are shown in Fig. 2b. They have been used as estimates of the parent background and lesion pdf's, i.e., of the pdf of the random variable x in the background and in the lesion areas, respectively, for the design of the associated L-filters following the procedure described in Section 2.2. Filters of order 3×3 were designed by calculating the ordered statistics from eqs. (10)–(13) and feeding the results to eqs. (8), (9) to estimate the quantities $\mathbf{R}$ and $\boldsymbol{\mu}$ needed in the computation of the filter coefficients (7). The integrals in (8) and (9) were replaced by sums over the range 0 to 63 since the image's grey levels lie in this interval.

A pair of L-filters have been designed by substituting s in (7) with the L_2 means of the two regions resulted by the segmentation procedure described above. The result of the L_2 mean based filter pair is shown in Fig. 4b. For comparison purposes, Fig. 4a shows the result of a single 3×3 L-filter designed in the same way, but by viewing the original image as stationary. It is seen in Fig. 4b that the speckle contrast, particularly in the background area, has been reduced, yielding a better discrimination of the lesion against the background. The corresponding filters' coefficients are given in Fig. 5. Observe that, although the background filter resembles the Rayleigh-optimum L-filters computed in [12], the optimum L-filter for the lesion area is very close to the median filter. This result is not unexpected in view of the Laplacian form of the histogram of the bright region shown in Fig. 2b.

Some classical filtering operators

The arithmetic mean and the median filters have also been used in our comparisons along with a number of well-known speckle filters:

1. *Homomorphic filter*: By taking the logarithm of $x = sn$, we obtain

$$\ln x = \ln s + \ln n \tag{16}$$

   thus transforming the problem to one of additive noise filtering. By averaging the logarithmized image the additive noise is suppressed and by exponentiating the result an estimate of s is obtained [21].

2. *Frost filter*: Following [10], Frost et al. [4, 3] derived a MMSE Wiener filter, on the basis of a first-order autoregressive model for the image signal, of the form

$$h(m, n) = K_1 \alpha e^{-\alpha \|(m,n)-(m_0,n_0)\|} \tag{17}$$

10

where (m_0, n_0) are the coordinates of the central pixel in the filter window, and

$$\alpha^2 = K_2 \left(\frac{\sigma_x^2}{\bar{x}^2} \right) + K_3 \tag{18}$$

with K_i, $i = 1, 2, 3$ being constants. In our experiments, the values 0.11, 18, and 0.5 were used for K_1, K_2, and K_3, respectively. This dependence of α on the coefficient of variation, $\sigma_x/\bar{x}$, makes the filter adaptive and allows edge information to be preserved.

3. *Sigma filter*: This filter consists in averaging not all pixel values in the current window but only those which fall into the interval having the central pixel level at its center and four times the standard deviation as its width. This way, edge smearing is avoided [13].

4. *Variable-length Median filter:* This is a median filter with a window size $2L+1$ by $2L+1$ calculated at each point from [16]

$$L = [K(1 - c\sigma_x^2/\bar{x})] \tag{19}$$

where the maximum window size is $2K + 1$ by $2K + 1$, c is a scaling constant (set here to 0.3), and $[a]$ denotes the integer part of a.

5. *Taylor filter:* The estimate of s is given by [19]

$$\hat{s} = x^a \tag{20}$$

where a is such that

$$E\{(s - x^a)^2\}$$

is minimum. By normalizing the data to near unity mean, x^a can be replaced by the Taylor approximation $x^a \approx 1 + a \ln x$, and the MMSE coefficient a is

$$a = \frac{E\{s \ln x\} - E\{\ln x\}}{E\{\ln^2 x\}} \tag{21}$$

All statistics involving x alone are obtained by their sample estimates within the filter window. The statistics involving s are derived from the latter and by using the model $x = sn$ with s and n assumed to be independent and n having unity expected value. Moreover, as in [19], it was seen to be necessary to use a manual bounding on the coefficients a ($-0.5 < a < 1.5$) to avoid the presence of spurious spots in the result.

Receiver Operating Characteristics

Some detection theoretic performance measures, namely, the probabilities of detection and false alarm, and the receiver operating characteristic [31] have also been used in our comparisons of the filters considered, to allow for numerically comparing their relative performance. The probability of detection (P_D) corresponds to the percentage of pixels of the image in the lesion area that have been correctly classified. The probability of false alarm (P_F) corresponds to the percentage of pixels belonging to the background of the image that were erroneously classified as belonging to the lesion. The probability of detection corresponding to a threshold chosen so that the probability of false alarm is approximately equal to 10% has been tabulated in Table 1 for the original image and its processed versions (linear interpolation was used, where necessary, to estimate P_D from its two closest values). The P_D values listed in Table 1 verify the enhanced detectability obtained by the filters that exploit the segmentation information, compared to their counterparts that are designed with the stationarity assumption. The low probabilities of detection for the median and the mean filters show their inadequacy for this kind of application.

Due to its strong dependency upon the operating point of the detector, the probability of detection P_D, for a fixed probability of false alarm P_F, may be proved an inadequate measure of detection performance. A more reliable figure of merit can be derived by examining the receiver operating characteristic (ROC), which is defined as the graph of P_D versus P_F. It has been extensively used in evaluating systems for medical diagnosis [28], because of its unique ability for providing a measure of accuracy, which is largely independent of decision bias. A single number that can completely characterize the whole ROC is the area under this curve and is included in Table 1. The comparison with respect to this figure of merit is again seen to be favorable for our method. The corresponding ROC curves are shown in Fig. 6.

An SNR measure

We have also compared the various filtering strategies from the viewpoint of the dispersion of the background and lesion pixels from the corresponding true sample means relatively to the dispersion in the original image. A measure of this relative dispersion, that could be called a signal-to-noise ratio, is defined for the lesion area as

$$\text{SNR}_L = \frac{\sum_{\text{lesion}} (x_i - m_L)^2}{\sum_{\text{lesion}} (\hat{x}_i - m_L)^2} \tag{22}$$

where x_i and $\hat{x}_i$ denote the values of the original and the filtered image, respectively, and m_L corresponds to the average level in the lesion that is estimated from the original image on the

12

basis of our a-priori knowledge of the lesion position, shape, and dimensions. The background SNR, SNR_B, is similarly defined. Table 2 summarizes the SNR values (in decibels) for our set of processed images.

Lesion contrast

The results presented thus far, demonstrate that our method outperforms all of the filters considered except for the Frost filter, which attains significantly higher values for the ROC area and the SNR compared to the segmentation-based approach. Nevertheless, as one can see by comparing the images in Fig. 4b and 7, these higher figures of merit for the Frost filter are at the cost of lower lesion contrast and an amount of blurring. This could be expected since, as noted in [15], Frost's filter cannot adequately smooth homogeneous areas and preserve heterogeneous areas at the same time. A quantitative verification of this point is provided by the following measure of lesion contrast [29]

$$C = \frac{m_L - m_B}{m_L + m_B} \tag{23}$$

where, as before, m_L and m_B denote the average levels in the lesion and the background, respectively. The contrast values for the original as well as the filtered images are tabulated in Table 3. Note that the Frost filter yields the lowest lesion contrast among all the filters studied here, with the highest value obtained through our method.

SNR imaging

A way of increasing the lesion contrast relative to the background is to subtract from an image its associated SNR image [32]. The SNR image is produced by a grey-level encoding of the point SNR evaluated at the corresponding pixels of the original image. The point SNR at pixel P is defined as the ratio of the sample mean to the standard deviation from this mean over a window $\mathcal{W}$ centered at that pixel [32]. That is,

$$\text{SNR}_P = \frac{\mu_P}{\sigma_P} \tag{24}$$

where

$$\mu_P = \frac{1}{N(\mathcal{W})} \sum_{i \in \mathcal{W}} x_i \tag{25}$$

and

$$\sigma_P = \left\{ \frac{1}{N(\mathcal{W}) - 1} \sum_{i \in \mathcal{W}} (x_i - \mu_P)^2 \right\}^{1/2}, \tag{26}$$

with $N(\mathcal{W})$ being the number of pixels enclosed in $\mathcal{W}$. The SNR image of the original image,

with $\mathcal{W}$ being a 15×3 window[4], is shown in Fig. 8a. The lesion is recognized as a dark disk-shaped region in this figure. The results of subtracting the SNR image from the L_2 mean based L-filtered images and the Frost filtered image are shown in Figs. 8b, 8c, and 8d, respectively. The image in Fig. 8c appears to permit a more accurate discrimination between the target and the background compared to Figs. 8b, 8d.

A real example

It is difficult to evaluate the performance of a speckle reduction technique with real data because the underlying scatterer distribution, and hence the ideal image, are not known. Nevertheless, the superioriry of our method over the single L-filtering can still be confirmed by inspection of the results from the application of the two methods to the real sector scan of Fig. 9. The result of the segmentation of this image by L_2 LVQ into 3 classes is depicted in Fig. 10. In Figs. 11a, b the outputs of the single L-filter and the L-filter triplet are shown. To demonstrate the effect of speckle filtering on the generation of the edge map of an image, we have applied the RGOA edge detector [34] to the original and filtered liver images. The results are shown in Fig. 12. It is obvious from Fig. 12a that, due to the presence of speckle, it is almost impossible to discern the edge structure of the original image. However, Figs. 12b, c show that edge detection becomes possible after a prefiltering stage. It should also be noticed that the segmentation-based L-filtering method allows for a cleaner edge map to be produced compared to its nonadaptive counterpart.

Before concluding this section we wish to make some remarks on the L_2 LVQ learning and filters' behavior in the conducted experiments. Neither longer training sessions nor NN training with more than two (three) classes could give us better classifiers (only two (three) of the classes were populated at the end). It seems, therefore, that the segmentations in Figs. 3 and 10 are the best we can obtain for these particular cases. It has also been found that the unbiased L-filter gives almost identical results with the unconstrained one.

4 Conclusions

We have presented a method for the suppression of speckle noise in ultrasonic B-mode images based on the idea of segmenting an image into stationary subimages prior to processing each

---

[4]Verhoeven et al. [32] have found that the lateral and the axial correlation sizes for the US B-mode image used are of the order of 15 and 3 pixels, respectively.

of them with a filter that is designed to be optimal for each particular subimage on the basis of the (statistical) information provided by the segmentation. Our method employs a modification of the LVQ algorithm based on the L_2 mean as a means of segmentation, while its filtering stage uses L-filters that are optimal in the MSE sense. Simulation experiments on an image of a tissue mimicking phantom and a real liver image verified the superiority of our approach to the single L-filter as well as to a number of commonly used speckle filters.

The L_2 LVQ training and the subsequent computation of more than one filters increase the computational complexity of our method to more than twice the computation needed in a conventional approach. However, this need not to be a problem since in medical applications the processing can be done off-line as pointed out in [16]. Moreover, the generalization capability of the LVQ NN, which has already been verified by simulations on SAR images [17], could be exploited to considerably reduce the computational load by using a single fixed network for segmentation, trained on a sufficiently large and representative sample of images.

In conclusion, we may say that the concept of "segmentation-based filtering," applied in the problem of speckle noise removal, provides us with methods of increased complexity but of high quality results since the filters can be matched in a natural manner to the local behavior of the image.

Acknowledgment

References

[1] A. C. Bovik, T. S. Huang, and D. C. Munson, "A Generalization of Median Filtering Using Linear Combinations of Order Statistics," *IEEE Trans. Acoustics, Speech, and Signal Processing,* vol. 31, no. 6, Dec. 1983, pp. 1342–1350.

[2] C. B. Burckhardt, "Speckle in Ultrasound B-Mode Scans," *IEEE Trans. Sonics and Ultrasonics,* vol. 25, no. 1, Jan. 1978, pp. 1–6.

[3] V.S. Frost, J.A. Stiles, K.S. Shanmugam, and J.C. Holtzman, "A Model For Radar Images and Its Application to Adaptive Digital Filtering of Multiplicative Noise," *IEEE Trans. Pattern Analysis and Machine Intelligence,* vol. 4, no. 2, March 1982, pp. 157–165.

[4] V.S. Frost, J.A. Stiles, K.S. Shanmugam, J.C. Holtzman, and S.A. Smith, "An Adaptive Filter for Smoothing Noisy Radar Images," *Proc. IEEE,* vol. 69, no. 1, Jan. 1981, pp. 133–135.

[5] J. W. Goodman, "Some Fundamental Properties of Speckle," *J. Optical Society of America,* vol. 66, no. 11, Nov. 1976, pp. 1145–1150.

[6] M. Halliwell, "Ultrasonic Imaging in Medical Diagnosis," *IEE Proc.,* vol. 134, Pt. A, no. 2, Feb. 1987.

[7] J. A. Kangas, T. K. Kohonen, and J. T. Laaksonen, "Variants of Self-Organizing Maps," *IEEE Trans. Neural Networks,* vol. 1, no. 1, March 1990, pp. 93–99.

[8] E. Kofidis, S. Theodoridis, C. Kotropoulos, and I. Pitas, "Segmentation-based L-Filtering of Speckle Noise in Ultrasonic Images," in *Nonlinear Image Processing V,* E. R. Dougherty, J. Astola, H. G. Longbotham, Eds., Proc. SPIE 2180, 1994, pp. 280–289.

[9] T. Kohonen, "The Self-Organizing Map," *Proc. IEEE,* vol. 78, no. 9, Sept. 1990, pp. 1464–1480.

[10] K. Kondo, Y. Ichioka, and T. Suzuki, "Image Restoration by Wiener Filtering in the Presence of Signal-Dependent Noise," *Applied Optics,* vol. 16, no. 9, Sept. 1977, pp. 2554–2558.

[11] C. Kotropoulos, X. Magnisalis, I. Pitas, and M. G. Strintzis, "Nonlinear Ultrasonic Image Processing based on Signal-Adaptive Filters and Self-Organizing Neural Networks," *IEEE Trans. Image Processing,* vol. 3, no. 1, Jan. 1994, pp. 65–77.

[12] C. Kotropoulos and I. Pitas, "Optimum Nonlinear Signal Detection and Estimation in the Presence of Ultrasonic Speckle," *Ultrasonic Imaging,* vol. 14, 1992, pp. 249–275.

[13] J.-S. Lee, "A Simple Speckle Smoothing Algorithm for Synthetic Aperture Radar Images," *IEEE Trans. Systems, Man, and Cybernetics,* vol. 13, no. 1, Jan/Feb. 1983, pp. 85–89.

[14] J.-S. Lee and I. Jurkevich, "Segmentation of SAR Images," *IEEE Trans. Geoscience and Remote Sensing,* vol. 27, no. 6, Nov. 1989, pp. 674–680.

[15] A. Lopes, R. Touzi, and E. Nezry, "Adaptive Speckle Filters and Scene Heterogeneity," *IEEE Trans. Geoscience and Remote Sensing,* vol. 28, no. 6, Nov. 1990, pp. 992–1000.

[16] T. Loupas, W.N. McDicken, and P.L. Allan, "An Adaptive Weighted Median Filter for Speckle Suppression in Medical Ultrasonic Images," *IEEE Trans. Circuits and Systems,* vol. 36, no. 1, Jan. 1989, pp. 129–135.

[17] S. P. Luttrel, "Image Compression Using a Multilayer Neural Network," *Pattern Recognition Letters,* vol. 10, July 1989, pp. 1–7.

[18] A. Macovski, *Medical Imaging Systems,* Prentice-Hall, Englewood Cliffs, N.J., 1983.

[19] C. R. Moloney and M. E. Jernigan, "Nonlinear Adaptive Restoration of Images with Multiplicative Noise," *Proc. ICASSP '89,* pp. 1433–1436.

[20] B. J. Oosterveld, J. M. Thijssen, and W. A. Verhoef, "Texture of B-mode Echograms: 3-D Simulations and Experiments of the Effects of Diffraction and Scatterer Density," *Ultrasonic Imaging,* vol. 7, 1985, pp. 142–160.

[21] A. V. Oppenheim, R. W. Schafer, and T. G. Stockham, Jr., "Nonlinear Filtering of Multiplied and Convolved Signals," *Proc. IEEE,* vol. 56, Aug. 1968, pp. 1264–1291.

[22] I. Pitas and A. N. Venetsanopoulos, *Nonlinear Digital Filters: Principles and Applications,* Kluwer Academic Publishers, Hingham MA, 1990.

[23] S. A. Rajala and R. J. P. de Figueiredo, "Adaptive Nonlinear Image Restoration by a Modified Kalman Filtering Approach," *IEEE Trans. Acoustics, Speech, Signal Processing,* vol. 29, no. 5, Oct. 1981, pp. 1033–1042.

[24] S. W. Smith and H. Lopez, "A Contrast-Detail Analysis of Diagnostic Ultrasound Imaging," *Med. Phys.,* vol. 9, no. 1, Jan/Feb. 1982, pp. 4–12.

[25] S. W. Smith, R. F. Wagner, J. M. Sandrik, and H. Lopez, "Low Contrast Detectability and Contrast/Detail Analysis in Medical Ultrasound," *IEEE Trans. Sonics and Ultrasonics,* vol. 30, no. 3, May 1983, pp. 164–173.

[26] A. Springub, D. Scheppelmann, and H.-P. Meinzer, "Segmentation of Multisignal Images with Kohonen's Self-Learning Topological Map," *Proc. Conf. Computer Analysis of Images and Patterns,* Dresden, Germany, Sept. 1991, pp. 148–152.

[27] R. N. Strickland, "Transforming Images into Block Stationary Behavior," *Applied Optics,* vol. 22, no. 10, May 1983, pp. 1462–1473.

[28] J. A. Swets et al., "Assessment of Diagnostic Technologies," *Science,* vol. 205, no. 4407, 24 Aug. 1979, pp. 753–759.

[29] J. M. Thijssen, B. J. Oosterveld, and R. F. Wagner, "Gray Level Transforms and Lesion Detectability in Echographic Images," *Ultrasonic Imaging,* vol. 10, 1988, pp. 171–195.

[30] M. Tur, K. C. Chin, and J. W. Goodman, "When is Speckle Noise Multiplicative?," *Applied Optics,* vol. 21, no. 7, April 1982, pp. 1157–1159.

[31] H. L. VanTrees, *Detection, Estimation, and Modulation Theory,* John Wiley & Sons, 1968.

[32] J. T. M. Verhoeven, J. M. Thijssen, and A. G. M. Theeuwes, "Lesion Detection by Echographic Image Processing: Signal-To-Noise Ratio Imaging," *Ultrasonic Imaging,* vol. 13, 1991, pp. 238–251.

[33] R. C. Waag, "A Review of Tissue Characterization from Ultrasonic Scattering," *IEEE Trans. Biomedical Engineering,* vol. 31, no. 12, Dec. 1984, pp. 884–893.

[34] M. R. Zaman and C. R. Moloney, "A Comparison of Adaptive Filters for Edge-preserving Smoothing of Speckle Noise," *Proc. ICASSP '93,* pp. V-77–80.

List of Figures

List of Tables

Input image   Classifier   L-filtering   Output image

Figure 1: Segmentation-based L-filtering.
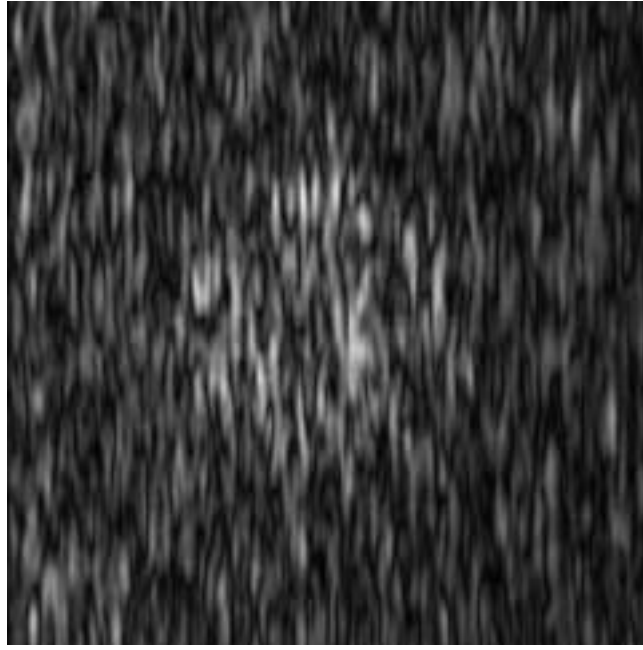
(a)
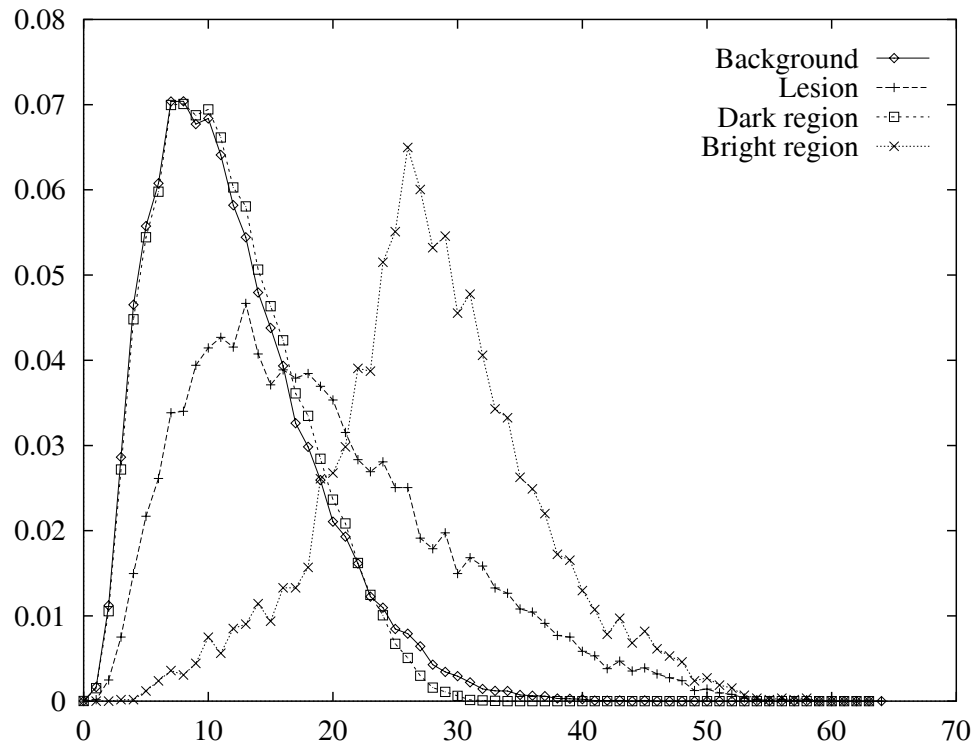
(b)

Figure 2: (a) US B-scan of a tissue simulating phantom. (b) Histograms of the lesion and the background areas in (a).
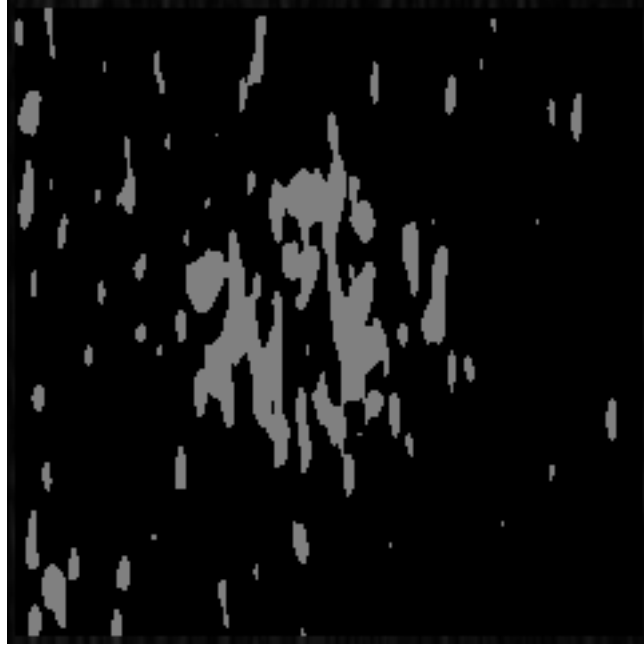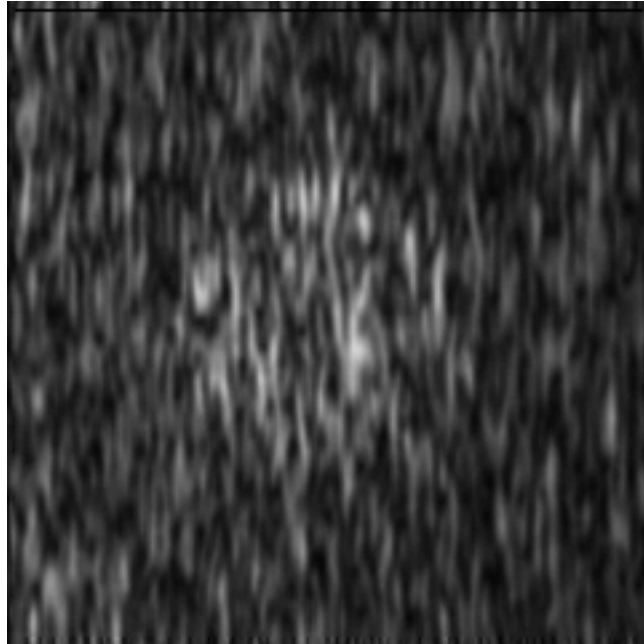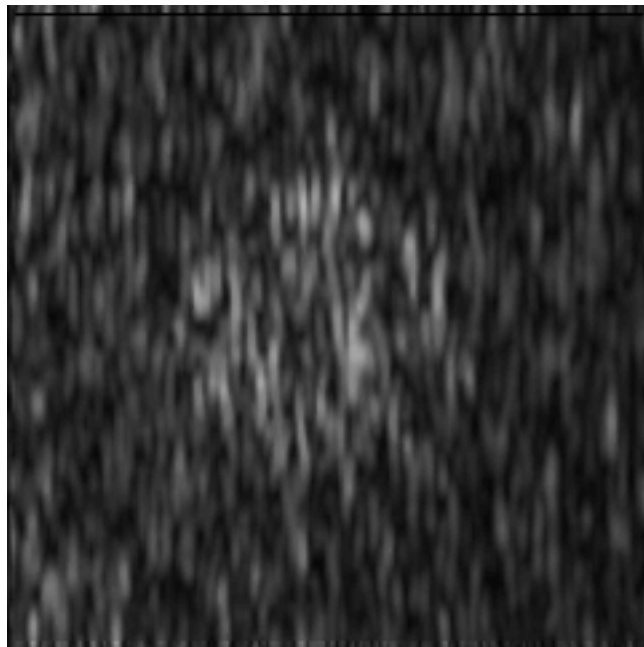
Figure 3: Result of the segmentation of Fig. 2a with the modified LVQ NN.

(a)

(b)

Figure 4: (a) Output of the single L_2-mean based L-filter. (b) Output of the L_2-mean based
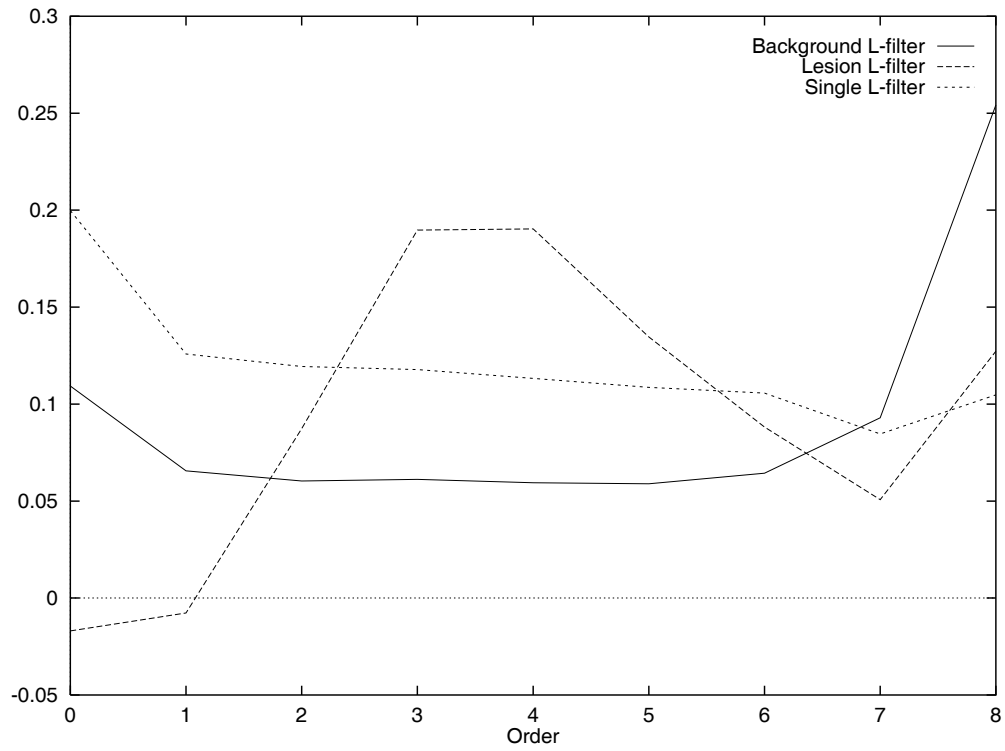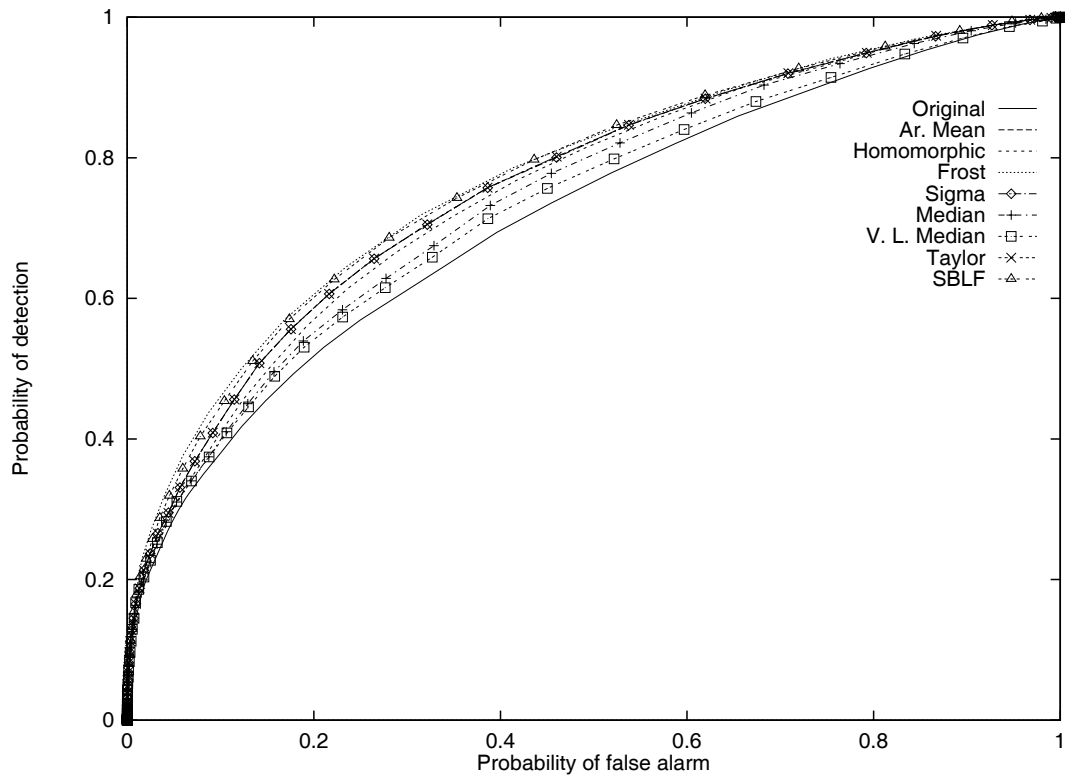L-filter pair.

Figure 5: L-filter coefficients.

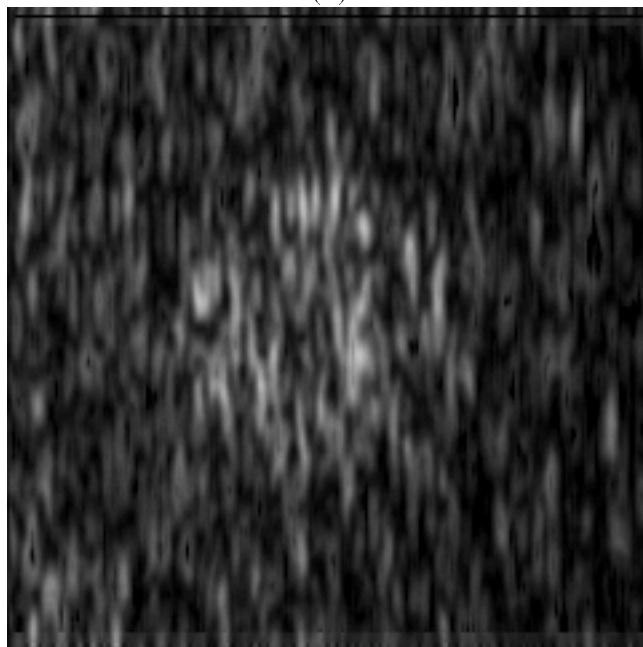Figure 6: Receiver operating characteristics.
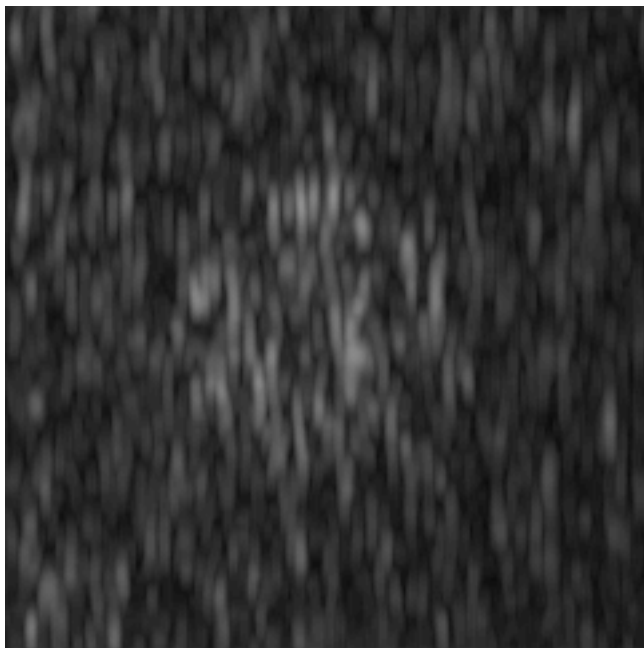
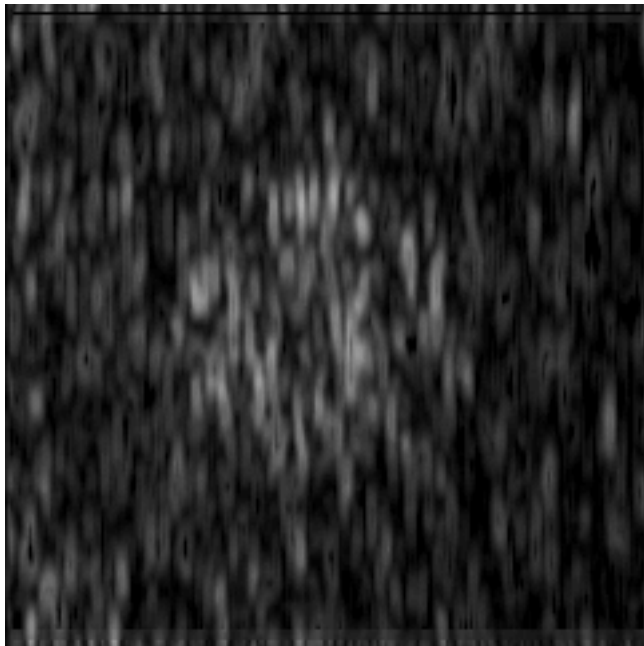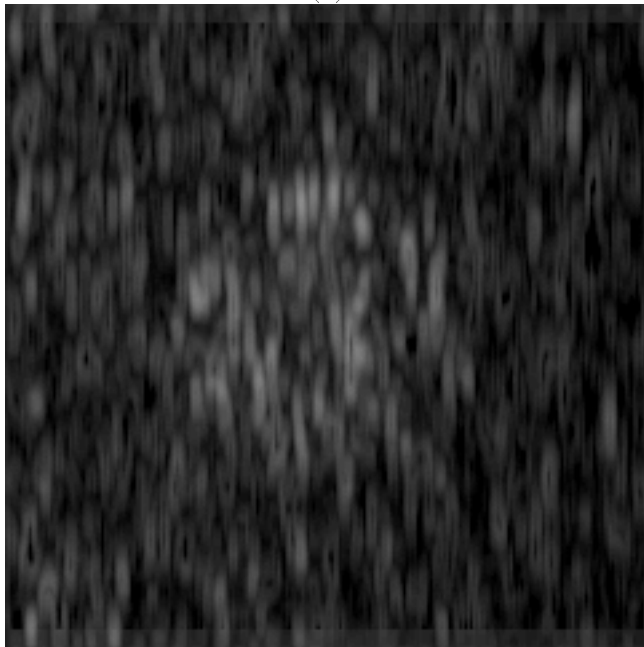Figure 7: Output of the Frost filter.
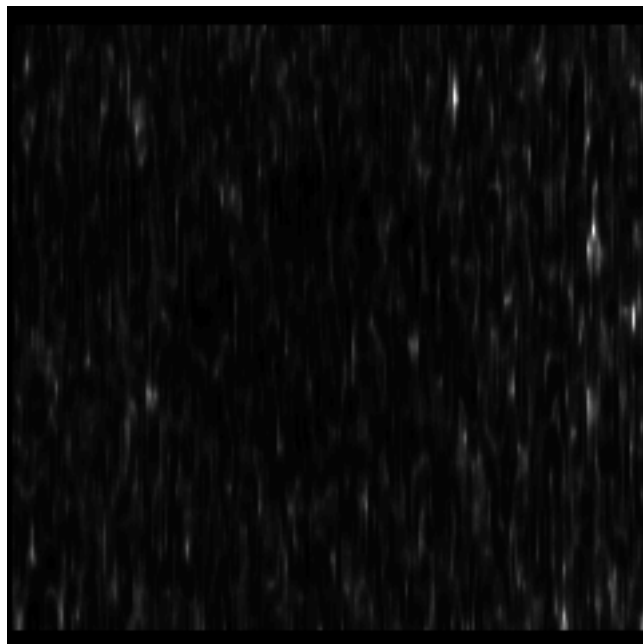
(a)

(b)

Figure 8: (a) SNR image of Fig. 2a. (b) Result of subtracting the image of (a) from that of Fig. 4a.

(c)

(d)

Figure 8: (cont'd) (c) Result of subtracting the image of (a) from that of Fig. 4b. (d) Result of subtracting the image of (a) from that of Fig. 7.
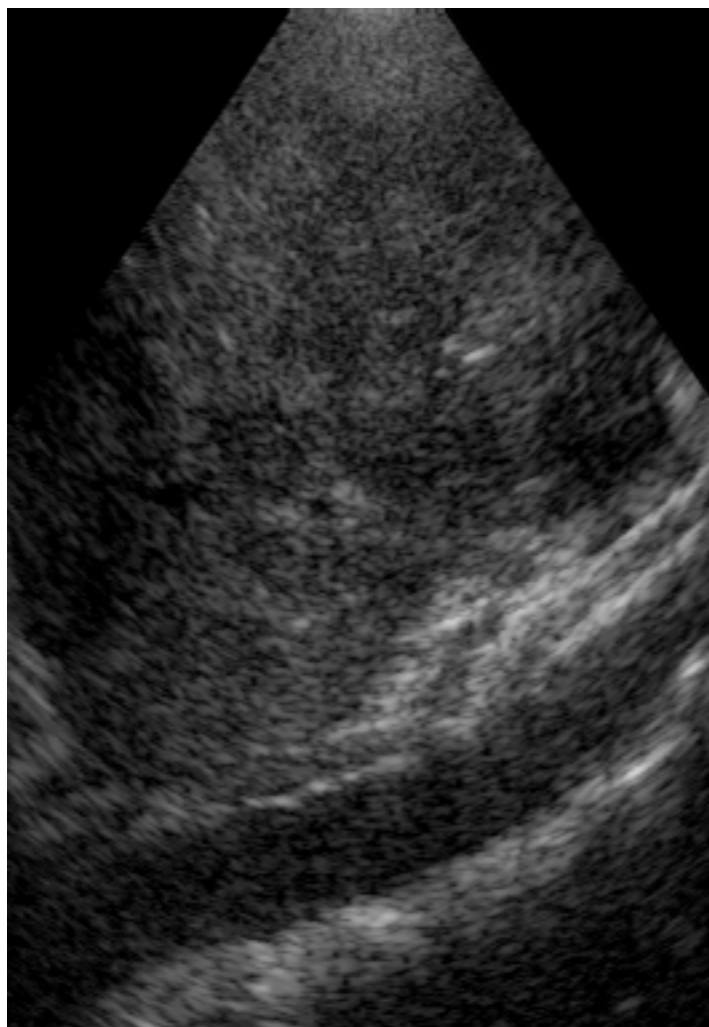
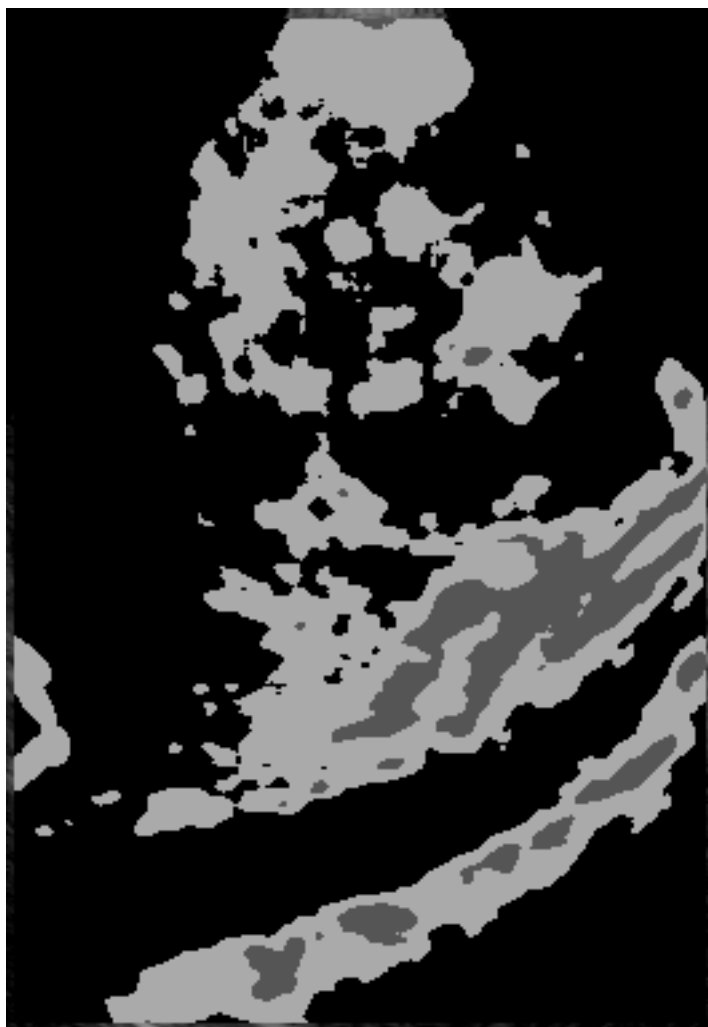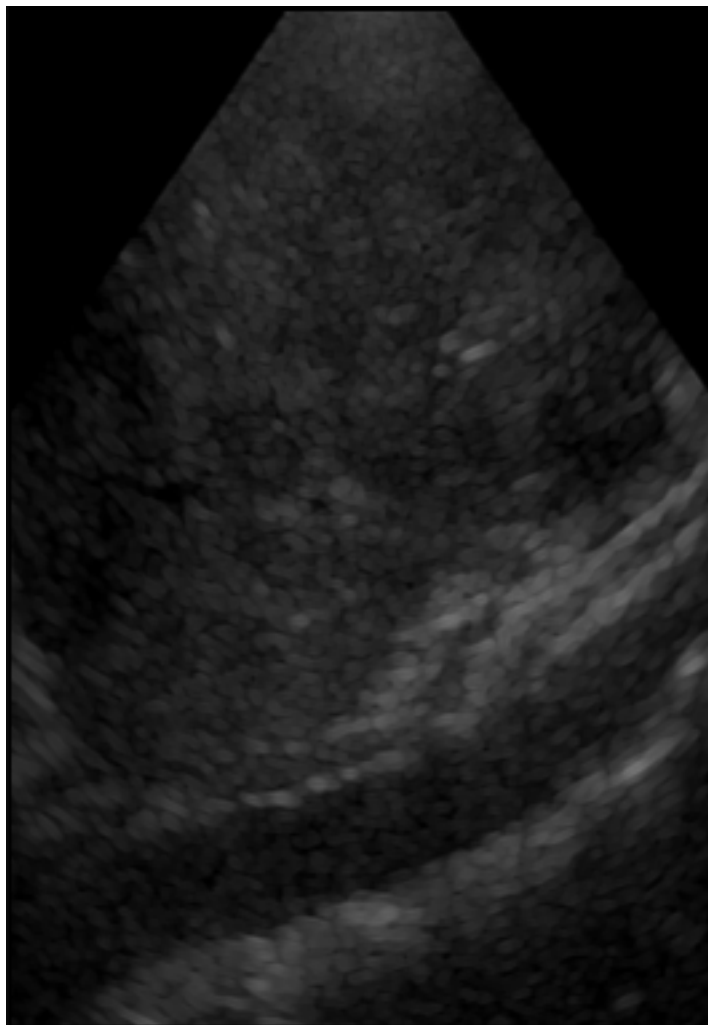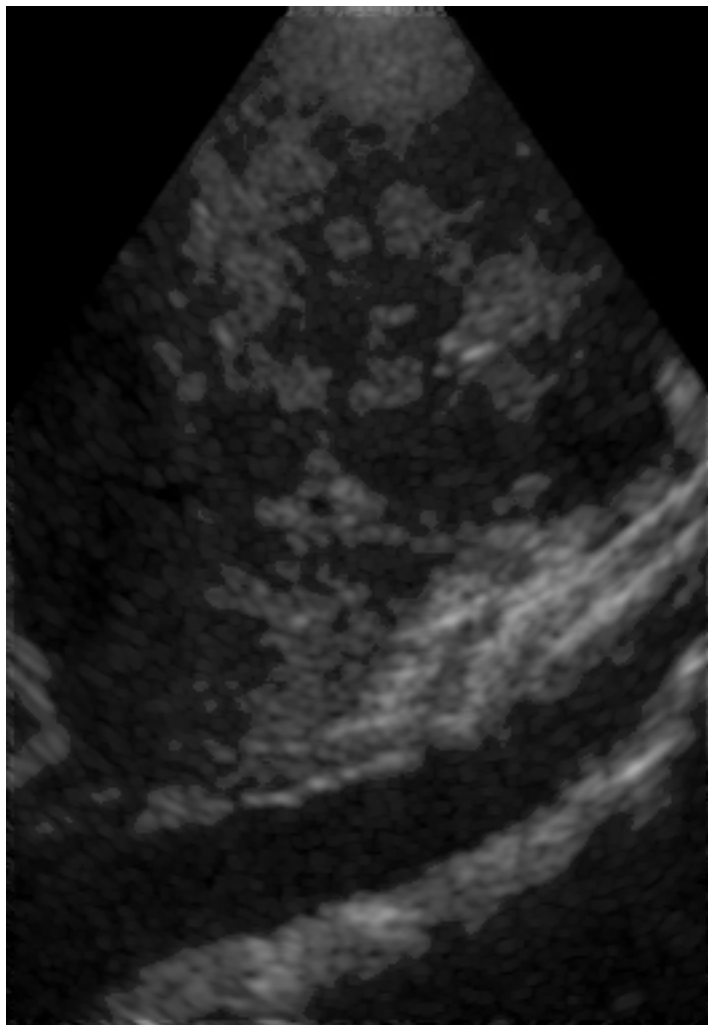Figure 9: US B-mode image of human liver.

Figure 10: Result of the segmentation of Fig. 9 with the L_2 LVQ NN.

(a)

Figure 11: (a) Output of the single L-filter.

(b)

Figure 11: (cont'd) (b) Output of the L-filter triplet.

(a)

Figure 12: (a) Edge map for the image of Fig. 9.

(b)

Figure 12: (cont'd) (b) Edge map for the image of Fig. 11a.

(c)

Figure 12: (cont'd) (c) Edge map for the image of Fig. 11b.

Table 1: Figures of merit for lesion detection on the simulated US B-mode image of Fig. 2a. (LF: single L-filter, SBLF: segmentation-based L-filter pair)

Method	P_F %	P_D %	Threshold	$\hat{P}_D$ %	Area under ROC
Image	8.198	35.04	22	37.981	0.717116
Thresholding	10.128	38.19	21		
Median	8.737	37.45	21	39.8838	0.743840
	10.60	41.04	20		
Ar. Mean	9.175	40.907	20	42.592	0.761905
	11.48	45.62	19		
Hom/phic	8.0845	36.91	20	40.88	0.754272
	10.051	40.987	19		
Frost	8.71	43.73	17	46.021	0.77281
	12.3	50.11	16		
Sigma	9.17	40.845	20	42.56	0.761576
	11.476	45.61	19		
V. L. Median	8.78	37.44	21	39.6336	0.731703
	10.68	40.854	20		
Taylor	9.175	40.9	20	42.592	0.761882
	11.48	45.61	19		
L_2 LF	8.674	38.8	21	41.77	0.758334
	10.7	43.343	20		
L_2 SBLF	7.838	40.3667	18	44.6027	0.764672
	10.406	45.3982	17		

Table 2: Relative dispersion resulting from processing the US B-mode image of Fig. 2a.

Method	SNR_B (dB)	SNR_L (dB)
Median	0.914986	0.885867
Arithmetic Mean	1.55226	1.5066
Homomorphic	1.56488	1.50149
Frost	4.59596	4.02855
Sigma	1.54537	1.49875
V. L. Median	0.812148	0.613674
Taylor	1.55216	1.5066
Single L-filter	1.09915	1.04087
Segmentation-based L-filter	2.28008	2.1488

Table 3: Lesion contrast for the image of Fig. 2a and its processed versions.

Method/Image	Contrast
Original	0.230441
Median	0.230212
Arithmetic Mean	0.230541
Homomorphic	0.231008
Frost	0.187298
Sigma	0.230571
V. L. Median	0.228513
Taylor	0.230541
Single L-filter	0.238434
Segmentation-based L-filter	0.238952